Opportunities for Chemical Engineering Thermodynamics in Biotechnology: Some Examples

Siddharth S. Dey and John M. Prausnitz*

Department of Chemical Engineering, University of California, Berkeley, California 94720-1462

Because of its generality, thermodynamics is applicable to all substances, including biomacromolecules. To illustrate how thermodynamics can contribute to biotechnology, each of six examples gives a brief summary of pertinent, previously published research. Each example indicates that familiar concepts in chemical engineering thermodynamics can be applied to contribute toward solution of a practical problem. These examples are discussed here to encourage thermodynamically oriented chemical engineers to devote their talents toward helping to advance industrial biotechnology.

Introduction

Because thermodynamics has a wide range of applicability, it is one of the cornerstones of chemical engineering, for example, in the formulation of energy balances in plant design and for calculation of phase equilibria for separation operations.

The last generation has produced an increasing extension of chemical engineering to include biotechnology. Can chemical engineering thermodynamics contribute to that extension? To illustrate that it can, this article presents six examples chosen from literature. While many more are available, these six examples serve to indicate that the thermodynamic concepts and tools developed for chemical engineering during the last 100 years are readily extended for aiding design and operation of biotechnological operations. In presenting these examples, no attempt is made to subject them to a critical analysis. They are given here primarily to encourage researchers in chemical engineering thermodynamics to turn their talents with confidence to assist the development of biotechnology.

It is appropriate to present these examples in the Festschrift dedicated to Stanley Sandler because he and his co-workers have been (and continue to be) pioneers in showing how chemical engineering thermodynamics can be applied to biomolecular engineering.

Example 1. Separation of Proteins and Viruses Using a Two-Phase Aqueous Micellar System

A common operation in biotechnology is the large-scale separation of desired proteins or viruses from the aqueous effluent of a bioreactor. Liquid−liquid extraction provides a well-established method that is easily scalable. However, because nonpolar solvents often denature biomolecules, conventional liquid−liquid extraction may not be suitable. Instead, as shown by Blankschtein and co-workers, separations of aqueous proteins or viruses can be achieved using a novel extraction system with two aqueous layers, one rich and the other poor in micelles.

In an aqueous solution of a surfactant, when the surfactant concentration exceeds its Critical Micellar Concentration (CMC), surfactant molecules self-assemble to form micelles that have hydrophobic tail groups forming the interior of the micelle and hydrophilic head groups in the aqueous solvent. Upon raising the temperature of a homogeneous micellar solution of nonionic surfactants, phase separation produces a two-phase aqueous system, with one phase rich and the other poor in micelles. To illustrate, Figure 1-1 shows the coexistence curve of an aqueous solution of the nonionic surfactant, $C_{10}E_4$, in the absence or presence of various proteins or viruses.[1] Nonionic surfactants are preferred over ionic surfactants because they more readily exhibit phase separation and do not bind to proteins or cause denaturation. At low concentrations of proteins or viruses, the phase diagram in Figure 1-1 is not changed. For this case, Blankschtein et al.[2] presented a theoretical equation for the protein (or virus) partition coefficient, wherein it was assumed that the interactions between biomolecules and nonionic surfactant micelles are primarily repulsive due to their finite molecular size.

The partition coefficient, K_z, where subscript z stands for the biomolecule (protein or virus), is defined as the ratio of the biomolecule concentration in the top ($C_{z,t}$, micelle-rich) phase to that in the bottom ($C_{z,b}$, micelle-poor) phase

$$K_z = \frac{C_{z,t}}{C_{z,b}} \tag{1-1}$$

For low biomolecule concentration and a nonionic surfactant, the partition coefficient is

$$K_z = \exp[-(\mu^o_{z,t} - \mu^o_{z,b}/k_BT)] \tag{1-2}$$

where k_B is the Boltzmann constant and $\mu^o_{z,t}$ and $\mu^o_{z,b}$ are standard-state chemical potentials of a biomolecule in the top and bottom phases, respectively. Because, by assumption, the biomolecules and the micelles interact only through repulsive excluded-volume interactions, the standard-state chemical potentials are a function of entropic factors only

$$\mu^o_{z,t} - \mu^o_{z,b} = -k_BT \ln\left(\frac{\Omega_t}{\Omega_b}\right) \tag{1-3}$$

where Ω_t and Ω_b represent the number of ways of placing a biomolecule in the top and bottom phases, respectively. Substitution of eq 1-3 into eq 1-2 gives

$$K_z = \left(\frac{\Omega_t}{\Omega_b}\right) \tag{1-4}$$

The number of ways to placing a biomolecule in each phase is proportional to the free volume available to the biomolecule;

* Corresponding author. E-mail: prausnit@cchem.berkeley.edu.

10.1021/ie1004916
Published on Web 07/13/2010

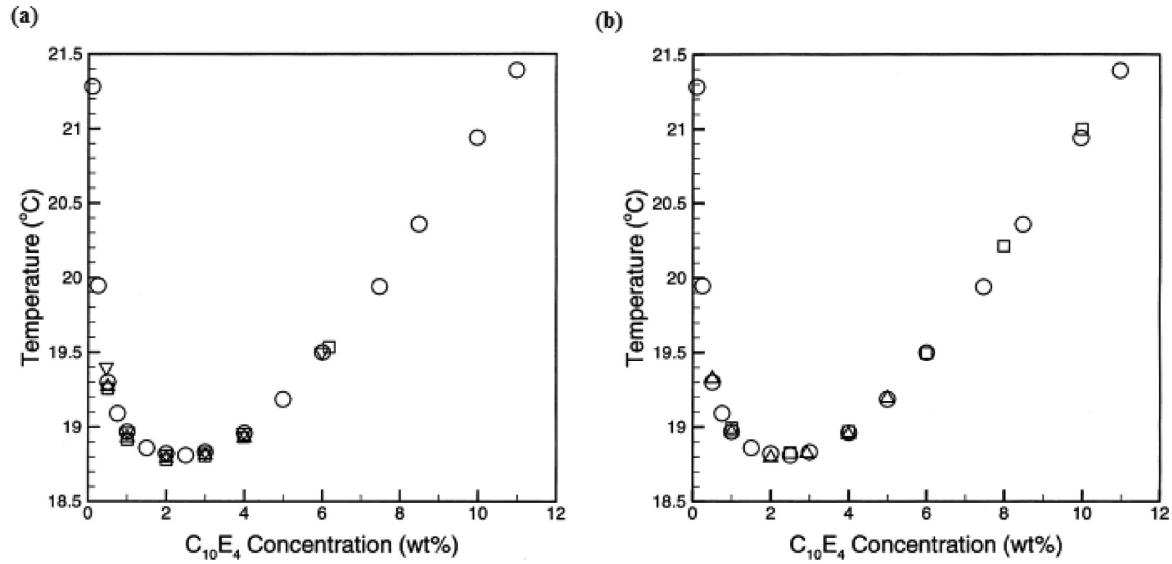

Figure 1-1. (a) Coexistence curves for aqueous $C_{10}E_4$ micellar solutions without protein (○) and with proteins cytochrome *c* (Δ), ovalbumin (∇), and catalase (□). (b) Coexistence curves for aqueous $C_{10}E_4$ micellar solutions without bacteriophage (○) and with bacteriophage P22 (Δ) and T4 (□). Adapted from ref 1.

this free volume can be estimated from molecular geometry. For two cases, the partition coefficient is then given by

$$K_z = \exp\left[-\varphi_t - \varphi_b\left(1 + \frac{R_z}{R_o}\right)^2\right] \text{ for spherocylindrical micelles} \tag{1-5}$$

$$K_z = \exp\left[-\varphi_t - \varphi_b\left(1 + \frac{R_z}{R_o}\right)^3\right] \text{ for spherical micelles} \tag{1-6}$$

where φ_b and φ_t are the volume fraction of surfactant in the bottom and top phases, respectively. R_z is the biomolecule radius, and R_o is the radius of a spherical micelle or the cross-sectional radius of a cylindrical micelle. These radii are obtained from crystallographic molecular-structure data.

Figure 1-2 shows experimental partition coefficients for different proteins as a function of temperature and protein radius; the experimental results are compared to those theoretically predicted based on the excluded-volume theory. Experimental and theoretical results are in good agreement. When K_z is less than 1, the protein preferentially partitions to the bottom (micelle poor) phase. Figure 1-3 shows similar plots for the partition coefficients for different viruses. There are significant differences between the experimental and predicted results, and theory predicts separation much better than that observed.

Two possible reasons for this discrepancy are:

1. The theory does not take into account attractive interactions between the virus and the micelles. Because cellular membranes are lipid bilayers, similar to micelles, parts of the outer viral envelope may interact with micelles, increasing the viral concentration in the micelle-rich phase, giving a higher partition coefficient than that predicted. However, Blankschtein et al.[3] showed that attractive interactions do not play a role in raising K_z.

2. Phase-separation equilibrium is not attained. Entrainment of small domains of the micelle-poor (virus-rich) phase in the micelle-rich (virus-poor) phase is responsible for the higher observed K_z.[4] Because entrained domains cause light scattering, the turbidity of the two phases was used to show the presence of entrainment that decreases with a declining volume ratio of the two phases.

While molecular-thermodynamic concepts suffice to explain the experimental results for proteins, an additional non-thermodynamic concept is needed to obtain a useful correlation of the experimental results. This example illustrates that in many practical cases in biotechnology, molecular thermodynamics is often helpful but not sufficient.

If x is the volume fraction of the micelle-poor domains in the micelle-rich phase and $C^{EV}_{v,rich}$ and $C^{EV}_{v,poor}$ are the concentration of virus in the micelle-rich and micelle-poor domain, respectively, the overall concentration of virus in the top micelle-rich phase is

$$C_{v,t} = (1 - x)C^{EV}_{v,rich} + xC^{EV}_{v,poor} \tag{1-7}$$

Rearranging gives

$$C_{v,t} = C^{EV}_{v,rich} + x(C^{EV}_{v,poor} - C^{EV}_{v,rich}) \tag{1-8}$$

Assuming that the virus partitions between the micelle-rich and micelle-poor domain according to the excluded-volume theory, $K^{EV}_v = (C^{EV}_{v,rich})/(C^{EV}_{v,poor})$.

Figure 1-3 shows that $K^{EV}_v \ll 1$ for viruses. Therefore

$$C_{v,t} \approx C^{EV}_{v,rich} + xC^{EV}_{v,poor} \tag{1-9}$$

Because $C^{EV}_{v,poor} \gg C^{EV}_{v,rich}$, even a small x can dramatically change the concentration of the virus in the top micelle-rich phase.

A similar analysis for the micelle-poor phase gives

$$\begin{aligned} C_{v,b} &= C^{EV}_{v,poor} + y(C^{EV}_{v,rich} - C^{EV}_{v,poor}) \\ &\approx C^{EV}_{v,poor}(1 - y) \end{aligned} \tag{1-10}$$

where y is the volume fraction of the micelle-rich domains in the micelle-poor phase.

Since y is small

$$C_{v,b} \approx C^{EV}_{v,poor} \tag{1-11}$$

The concentration of virus in the micelle-rich and that in the micelle-poor phase give a modified equation for the partition coefficient

$$K_v = K^{EV}_v + x(1 - K^{EV}_v) \tag{1-12}$$

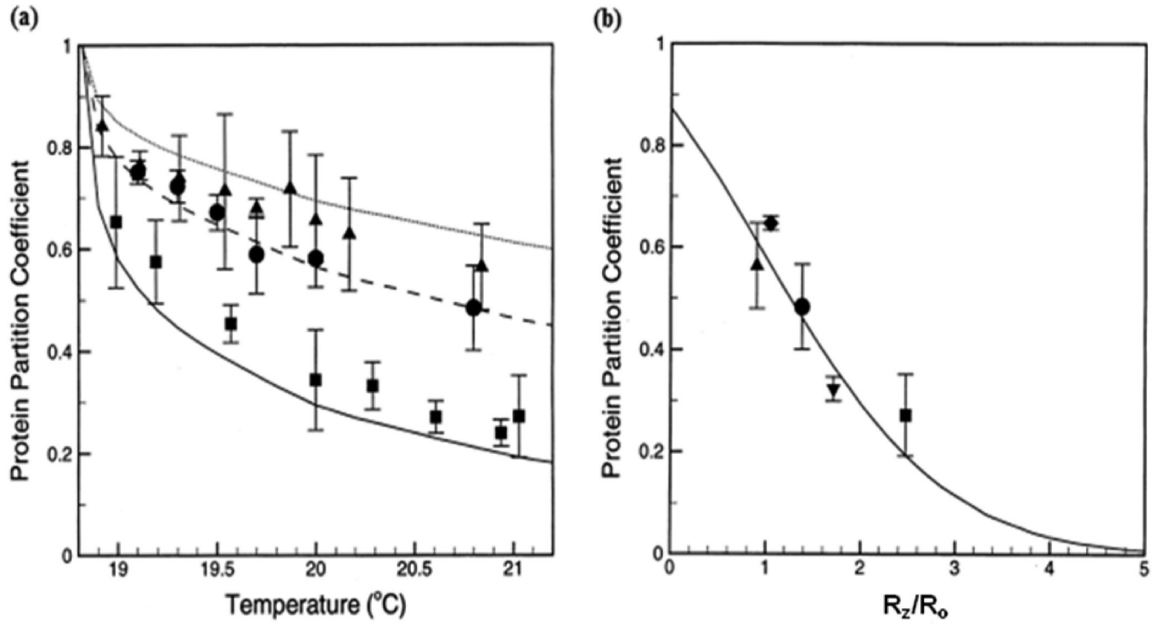

Figure 1-2. (a) Partition coefficients as a function of temperature for proteins cytochrome *c* (▲), ovalbumin (●), and catalase (■). (b) Partition coefficients as a function of R_z/R_o for proteins cytochrome *c* (▲), ovalbumin (●), bovine serum albumin (▼), soybean trypsin inhibitor (♦), and catalase (■). The error bars represent 95% confidence intervals. The predicted correlations are shown by continuous curves. Adapted from ref 1.

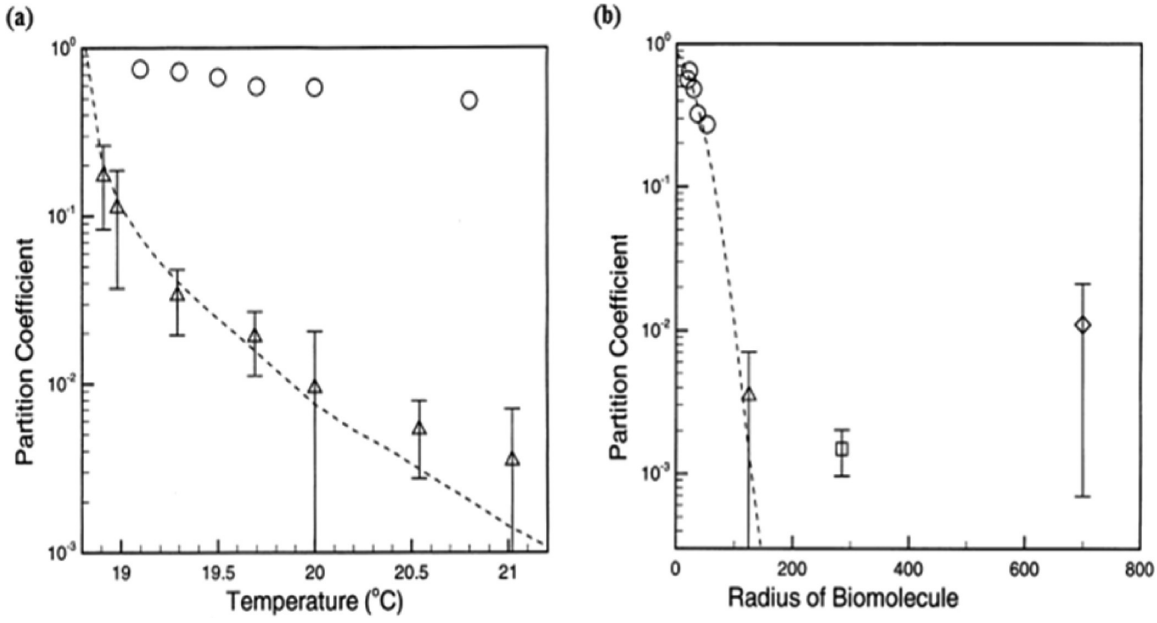

Figure 1-3. (a) Partition coefficients as a function of temperature for bacteriophage ϕX174 (Δ) compared with those for the protein ovalbumin (○). (b) Partition coefficients as a function of radius of the biomolecule for viruses ϕX174 (Δ), P22 (□), and T4 (◊) compared with different proteins (○). The error bars represent 95% confidence intervals. The predicted correlations are shown by continuous curves. Adapted from ref 1.

Figure 1-4 shows good agreement for the predicted and experimental partition coefficients for a virus.

Figures 1-3 and 1-4 show that, prior to interpreting data using thermodynamic analysis, it is of utmost importance to ensure that equilibrium has been attained; in the absence of equilibrium, semi-empirical corrections are necessary. Nevertheless, thermodynamic analysis can provide useful guidance; modified thermodynamic analysis of the two-phase aqueous micellar system described above may provide a useful method for designing a process for separating therapeutic proteins and, perhaps, for purification of viruses for large-scale production of gene delivery viral vectors.

This example shows that, in practice, thermodynamic analysis can sometimes provide only a partial explanation of the observed phenomena. For a more complete analysis, it may be necessary to consider other factors, in this case, entrainment.

Example 2. Isothermal Titration Calorimetry for AIDS Drug Development

Much effort has been directed toward finding drugs to help victims of the AIDS epidemic caused by the HIV virus. Thermodynamics makes a contribution to that effort through thermodynamic interpretation of experimental calorimetric−titration data.

As shown in Figure 2-1, after the HIV virus infects a human cell, a series of steps produces replication of HIV. The infected cell expresses a polyprotein and an HIV protease; the role of

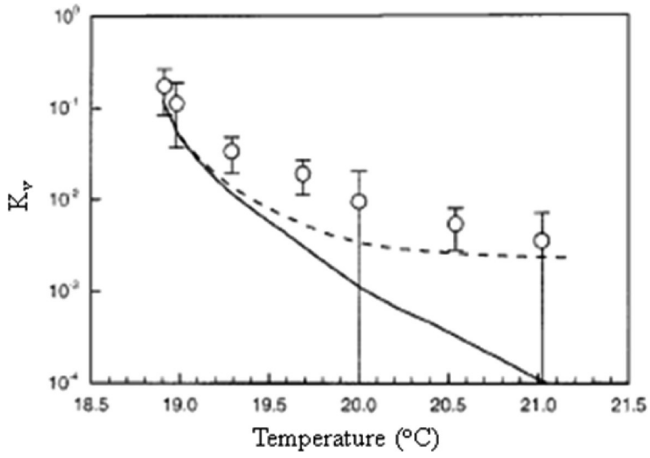

Figure 1-4. Improved prediction of the partition coefficients when entrainment is also considered. Experimentally determined partition coefficients for bacteriophage ϕX174 are shown by circles (○). The solid and dashed lines correspond to partition coefficient prediction without and with entrainment. The error bars represent 95% confidence intervals. Adapted from ref 4.

the protease is to cleave the polyprotein. The cleaved proteins assemble to form a new HIV virus.

An effective strategy to prevent formation of a new virus is provided by introducing a drug that deactivates the HIV protease. This drug, called a protease inhibitor, prevents cleavage of the polyprotein, as indicated in Figure 2-2.

Deactivation of a protease by an inhibitor can be described by a traditional lock-and-key mechanism indicated in Figure 2-3. The inhibitor must have the correct shape to fit into the active site of the HIV protease; here, the inhibitor is the "key" that must fit into the protease "lock".

However, because of mutations, the active site of an HIV protease can exist in a variety of forms, as shown schematically in Figure 2-3; the shape of the active site of the wild type (the lock) is represented by a cross, while for the mutant the shape of the lock is represented by a hexagon. We seek an inhibitor (the key) that is sufficiently flexible such that it "fits" into both types of locks. We need a drug (the key) that can bind not only to the active site of the wild-type protease but also to that of its mutant. Thermodynamics can help to identify the best drug candidates.

To illustrate, Figure 2-4 shows two possible drug candidates, 1 and 2. Drug 2 has better adaptability than drug 1 because, compared to drug 1, it has asymmetrical functionality; the toluene group has less symmetry than the tertiary butyl group, as indicated by oval circles. Further, drug 2 is more flexible because it has two rotating bonds, while drug 1 has only one, as indicated by dashed arrows. Asymmetry and flexibility provide the drug with additional conformations that can adapt to a mutant HIV binding site.

Toward obtaining a quantitative measure of drug efficacy, Ohtaka and Freire[5] use thermodynamic analysis of data from isothermal titration calorimetry (ITC).

Let A stand for the HIV protease and B for the (drug) inhibitor. We define a dissociation constant K_d and its reciprocal, association constant K_a, where subscript *a* stands for association and subscript *d* for dissociation.

$$K_d = \frac{[A][B]}{[AB]};\ K_a = \frac{[AB]}{[A][B]};\ K_a = (K_d)^{-1} \qquad (2\text{-}1)$$

where [ ] stands for concentration in water. For good drug efficacy, we want K_d to be small or, equivalently, K_a to be large.

In the reaction A + B → AB, the binding of A (protease) and B (inhibitor) is determined by standard-state enthalpy ΔH^o and entropy ΔS^o through the thermodynamic relation

$$-RT \ln K_a = \Delta G^o = \Delta H^o - T\Delta S^o \qquad (2\text{-}2)$$

where superscript o indicates a standard state.

Isothermal titration calorimetry (ITC) provides experimental results for K_d (or K_a) and ΔH^o. From these results, we calculate ΔG^o and ΔS^o.

Figure 2-5 shows experimental results for ΔG^o, ΔH^o, and $-T\Delta S^o$ for a first-generation set of 12 drug candidates where the protease is of the wild-type.

In Figure 2-5, the first generation of drugs contains molecules that are relatively rigid (not flexible). Within the active-site pocket of the protease, rigid molecules cannot interact strongly with the functional groups of the protease, and therefore, for these drugs, ΔH^o is not favorable; in some cases, while negative, the absolute value is small, and in other cases, most unfavorable, ΔH^o is positive. However, $-T\Delta S^o$ is favorable because upon

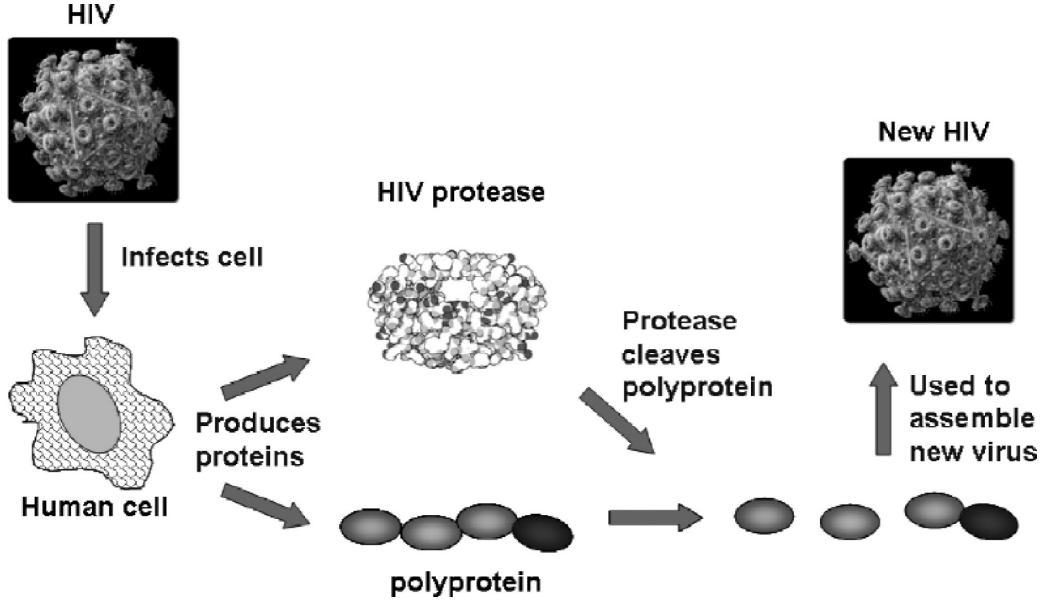

Figure 2-1. Schematic overview of viral reproduction showing the role of the HIV protease in synthesizing new viruses.

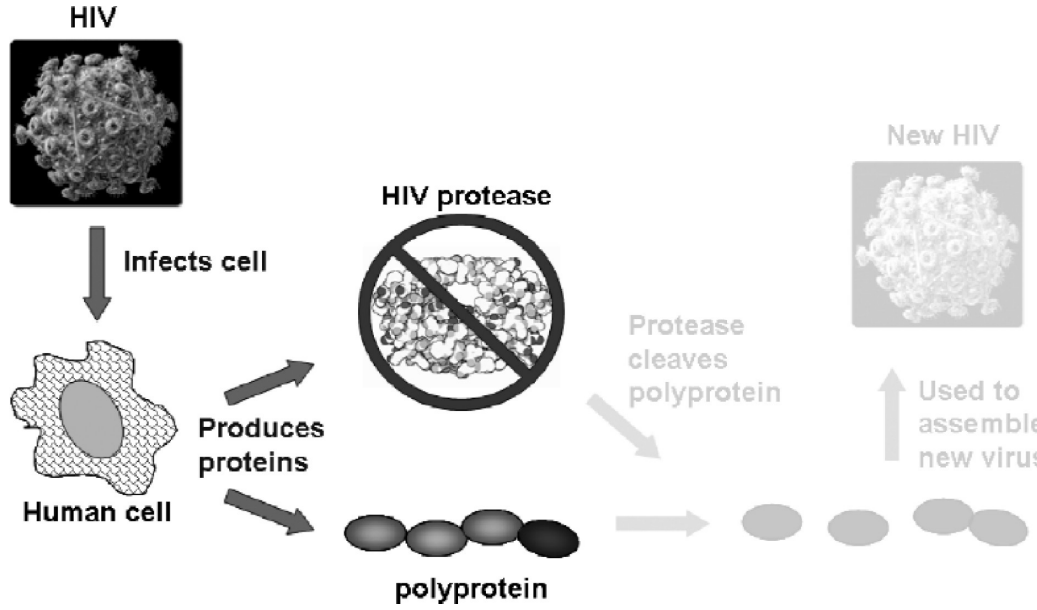

Figure 2-2. One method for reducing viral production is to inhibit the HIV protease to prevent it from cleaving the polyproteins as required for assembly of new viruses.

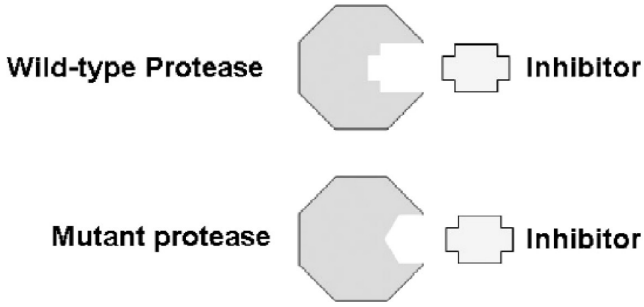

Figure 2-3. Traditional lock-and-key mechanism of inhibitor design requires shape complementarity between the active site on the HIV protease (lock) and the inhibitor molecule (key). A rigid key (as shown here) becomes ineffective when the protease mutates (bottom). It is advantageous to design an adaptable inhibitor (key) that can fit both the wild-type and the mutant protease (lock).

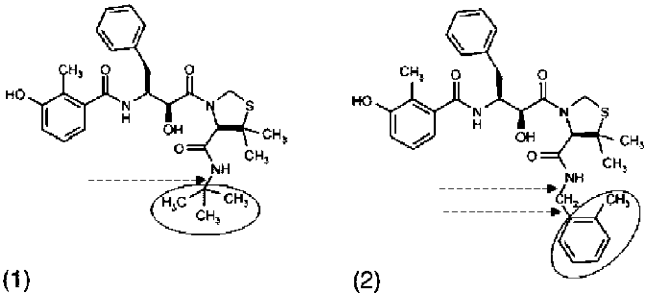

Figure 2-4. Of the two inhibitor drug candidates shown, 2 has greater adaptability than 1 due to its asymmetric functionality (circles) and additional rotatable bond (two instead of one, as indicated by the dashed arrows). Adapted from ref 5.

binding the hydrophobic drug releases hydrated water molecules with a subsequent desirable gain in entropy.

Because rigid drug molecules do not have as much adaptability to mutant proteases as flexible drug molecules, second-generation inhibitors are relatively flexible drugs. As shown in Figure 2-5, these drugs show a favorable (negative) ΔH^o, but $-T\Delta S^o$ is now less favorable because of what is called the entropic penalty: when a flexible key enters a confining lock, it loses not only translational degrees of freedom (as does a rigid key) but also rotational degrees of freedom. These losses in freedom produce a decrease in entropy; because this decrease is unfavorable, flexible drugs exhibit a greater entropic penalty (smaller $|-T\Delta S^o|$) than rigid drugs. However, the favorable trade-off for the unfavorable entropic penalty is a stronger binding interaction (i.e., a large negative ΔH^o). Figure 2-5 suggests that drugs 11 and 12 are best because ΔH^o and ΔG^o are both large and negative, as desired.

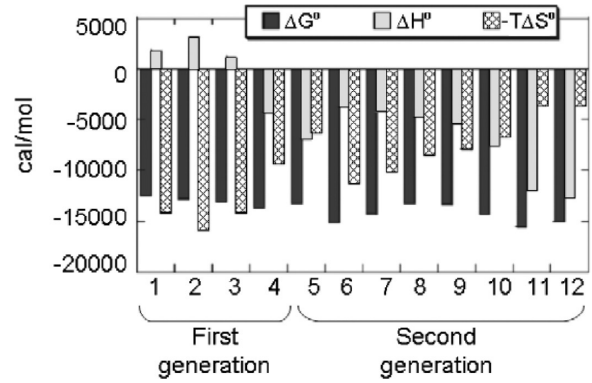

Figure 2-5. ITC data for protease inhibitors in clinical use (1−7) and several experimental inhibitors (8−12). The first-generation drugs are less adaptable than the second-generation drugs. Inhibitors 11 and 12 are good because they have large and negative ΔG^o and ΔH^o. Adapted from ref 5.

Because protease mutations are common, we seek an inhibitor that is not only effective for the wild-type protease but also adaptive to at least some of its mutants.

Figure 2-6 shows ITC results for a series of inhibitors interacting with the wild type and with a particular mutant. The ordinate, on a logarithmic scale, shows the dissociation constant K_d; we want K_d to be small not only for the wild type but also for the mutant.

Figure 2-6 shows the importance of having a large, negative ΔH^o. The more adaptive second-generation drugs (e.g., inhibitors 11and 12) have the smallest dissociation constant for both the wild-type and for the mutant HIV protease. In Figure 2-5, results for the wild-type protease indicate that inhibitors 11and 12 are best because they have two desirable features; both ΔG^o and ΔH^o are negative and large. However, Figure 2-6 shows that,

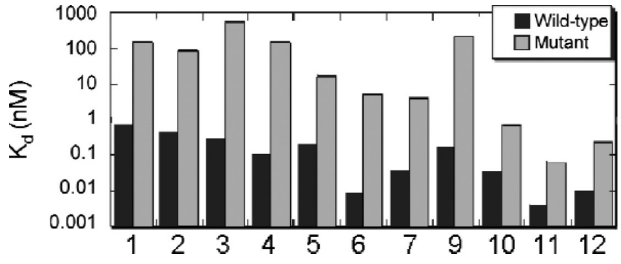

Figure 2-6. Dissociation constant for 10 inhibitors interacting with the wild-type HIV protease and one mutant form of the protease (data for inhibitor 8 omitted). Inhibitor 11 is superior to inhibitor 12 because K_d is smaller for both the wild-type and the mutant protease. Adapted from ref 5.

while inhibitors 11and 12 are good for the wild-type protease inhibitor 11 is superior for inhibiting the mutant protease. Figure 2-6 suggests that drug 11 is better than drug 12.

For a flexible inhibitor (as opposed to a rigid inhibitor), we must pay the price of a larger entropic penalty; this penalty is undesirable because it lowers the absolute value of a negative ΔG^o. We want an inhibitor that is flexible enough to give a large negative ΔH^o and also useful for a protease mutant. The inhibitor should not be too flexible lest the entropic penalty become too large. This example shows that thermodynamic studies are useful for guidance toward identifying an optimum HIV inhibitor.

Example 3. Protein Purification: Effect of Salt on the Phase Diagram for an Aqueous Solution of Globular Proteins

In biotechnology, initial separation of a target protein from a bioreactor broth is often achieved by adding a salt to induce precipitation. To provide guidance for attaining the desired results, we require a pertinent phase diagram, i.e., a plot of temperature vs protein concentration (or its equivalent, protein density) designated by number density ρ. A common way to express protein density is provided by the protein packing fraction

$$\eta = \frac{\pi}{6}\rho\sigma_p^3$$

where σ_p is the protein diameter.

While a bioreactor broth may contain several types of biomacromolecules in addition to other small solutes (e.g., a buffering salt), attention here is focused on a target protein, neglecting the presence of other biomacromolecules. The effect of other small solutes is included in the potential of mean force.

For fluid−solid equilibria, at constant temperature T, the essential equations of equilibrium are

$$\mu^F(\eta^F, T) = \mu^S(\eta^S, T) \quad (3\text{-}1)$$

$$p^F = p^S \quad (3\text{-}2)$$

where μ^F is the chemical potential of the protein in the fluid phase; μ^S is the chemical potential of the protein in the solid phase; and p is pressure.

At constant temperature, pressure p and chemical potential μ are related to density ρ by well-known thermodynamics; both are derived from an expression for Helmholtz energy A as a function of temperature and ρ (or η), as discussed in numerous textbooks.

A convenient procedure for calculating A^F for the fluid and A^S for the solid is to use the first-order Barker−Henderson perturbation theory, one for the fluid phase and another for the solid phase, as discussed, for example, by Tavares and Prausnitz.[6,7] For each phase, the chemical potential is obtained from two contributions, a hard-sphere (hs) term and a perturbation term (P)

$$\mu = \mu^{hs} + \mu^P \text{ and } P = P^{hs} + P^P$$

For the fluid phase, μ^{hs} is obtained from the Carnahan−Starling equation of state. For the solid phase, μ^{hs} is obtained from the equation of state proposed by Velasco and Mederos.[8]

To calculate μ^P, we need an expression that provides information concerning the protein−protein interaction in the aqueous solution and in the solid precipitate. That expression is the potential of mean force $W(r)$ where r is the center-to-center distance between two quasi-spherical (globular) protein particles. To a reasonable approximation, as suggested by colloid theory, this potential of mean force contains the following contributions

$$W(r) = W(r)^{hs} + W(r)^{el} + W(r)^{att} + W(r)^{ions} \quad (3\text{-}3)$$

where el refers to electrostatic forces and att refers to attractive (dispersion) forces.

W^{hs} depends on the reduced distance r/σ_p. The potential of mean force depends on the concentration and nature of the precipitating salt.

When a salt is present in the aqueous protein solution, W^{el} depends on r/σ_p, σ_s, q_p, q_s, D, and T where σ_s is the salt diameter, q_p is the protein charge, q_s is the salt charge, and D is the dielectric constant of water. Protein charge q_p depends on pH.

W^{att} depends on r/σ_p, on H, and on a new expression, φ(ions). Here, H is the Hamaker constant that reflects dispersion (van der Waals) forces between two aqueous protein particles in a salt-free medium; $W(r)^{ions}$ provides the contribution to protein−protein attractive forces due to dispersion forces arising from van der Waals interactions between the ions and between the ions and the protein particles. It is this function, φ(ions), that can explain the well-known Hofmeister series. (The Hofmeister series lists ions in decreasing order in their ability to salt-out dissolved proteins.) While the Hofmeister series was discovered empirically more than 100 years ago, its quantitative (theoretical) formulation was derived only recently by Ninham and co-workers[9] and by Tavares et al.[10] In this formulation, the function φ(ion) depends on the aqueous polarizabilities of the protein and the salt ions. An alternate explanation for the Hofmeister effect is based on selective hydration as discussed, for example, by Collins et al.[11] and by Hummer and Garde et al.[12−14]

For typical protein solutions, a decrease in temperature may show two fluid phases because high temperature encourages random mixing. In some cases, these fluid phases may be metastable. At constant temperature, the compositions of these two phases (′ and ″) are related by:

$$\mu^{F'}(\eta^{F'}, T) = \mu^{F''}(\eta^{F''}, T) \quad (3\text{-}4)$$

$$p' = p'' \quad (3\text{-}5)$$

At a fixed temperature, we have two unknowns, viz., the densities of the two equilibrium phases. They are obtained by simultaneous solution of eqs 3-1, 3-2, 3-4, and 3-5.

Figure 3-1 shows the important effect of the salt's anion for lysozyme equilibria. NaCl and NaI show qualitatively similar behavior; we see a fluid−fluid region with an upper critical point on the left side and a fluid−solid region on the right. However, because the polarizability of the iodide ion is larger than that

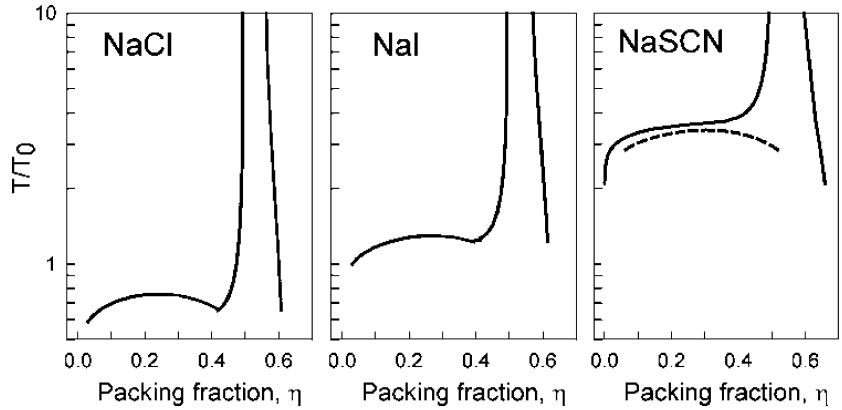

Figure 3-1. Three calculated phase diagrams for lysozyme at pH 4.3 where the lysozyme charge, $q_p = +10$. Each diagram is for an aqueous lysozyme solution containing a sodium salt with concentration 0.2 M. The protein diameter, σ_p, is 3.3 nm. $T_0 = 298$ K. In conventional theory, where the polarizabilities of protein and salt ions are neglected, these three phase diagrams are identical.

of the chloride ion and because higher polarizabilities increase attractive forces, the critical temperature for NaI is appreciably higher than that for NaCl.

For NaSCN, we obtain a phase diagram that is qualitatively different from those for NaCl and NaI because the polarizability of the SCN ion is larger than those for the iodide and chloride ions. For NaSCN, we do not have a stable fluid−fluid region; only fluid−solid equilibria are thermodynamically stable. However, in addition to fluid−solid equilibria, we also calculate metastable fluid−fluid equilibria, consistent with experiment. The calculations show a metastable region (dashed line where $\mu^{F'} = \mu^{F''}$), where superscript $'$ refers to a dilute aqueous lysozyme solution and superscript $''$ refers to a concentrated aqueous lysozyme solution.

For solutions containing NaCl or NaI, fluid−fluid equilibria are stable. However, for lysozyme solutions containing NaSCN, $\mu^{F'}$ and $\mu^{F''}$ are larger than the corresponding μ^{s} at the same temperature. For this case, the calculated (and observed) fluid−fluid equilibria are metastable.

Because of the larger polarizability of the SCN ion, these ions are attracted more strongly to the positively charged lysozyme, reducing the repulsive forces between lysozyme particles. Thus, for lysozyme, at pH 4.3, NaSCN is a more effective precipitating salt than NaCl or NaI. The thermodynamic discussion outlined here may provide initial guidance for designing an effective precipitation process.

Example 4. Liquid−Liquid Equilibria Suggest a Possible Method to Prevent Cataracts in the Human Eye

Cataracts are formed by aggregation of proteins in the eye. Small assemblies of protein molecules produce mesoscopic particles that interfere with normal vision. To obtain a quantitative description of protein aggregation, it is useful to establish a phase diagram that gives the coexistence curve (binodal) for liquid−liquid equilibria; phase separation indicates aggregation. As shown by Benedek et al.,[15] the coexistence curve can be modified by a small amount of an additive that lowers the upper critical solution temperature below body temperature. By preventing protein aggregation, it is possible to prevent formation of cataracts.

Condensation of proteins results in eye-lens turbidity that can be quantified by measuring the intensity of light scattered by the lens. As shown by Thurston et al.,[16] the intensity of light scattered (I_{scatt}) is given by

$$I_{scatt} = I_0 \exp(t/\Delta Z) \tag{4-1}$$

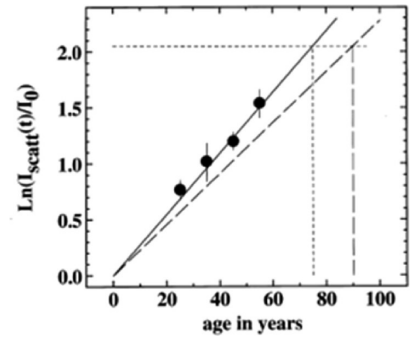

Figure 4-1. Intensity of light scattering from eye vs the age of a person. Straight solid line indicates experimental data. Dotted line shows a hypothetical case where the time constant ΔZ is increased by 20%, possibly by the addition of a pharmacological agent. This rise in ΔZ increases the age where 50% of the population would develop cataracts from 75 to 90 years. Adapted from ref 15.

where I_o is the intensity of incident light; t is the age of a person; and ΔZ is a time constant obtained from experimental data. Figure 4-1 shows that by addition of a cataract inhibitor, a 20% increase in ΔZ can prevent the onset of cataracts. Thermodynamic studies can establish the effect of an inhibitor on the binodal curve.

Calf eye-lens proteins have an amino acid sequence similar to those in the human eye-lens. These proteins, called γ-Crystallins, have been studied extensively. They have been classified into two major groups based on their aqueous critical-solution temperatures (T_c):

1. High-T_c proteins: γ_{IIIa} (γ_C) and γ_{IVa} (γ_E) Crystallins with ($T_c \approx 38$ °C).

2. Low-T_c proteins: γ_{II} (γ_B) and γ_{IIIB} (γ_D) Crystallins with ($T_c \approx 5$ °C).

Figure 4-2 shows binary aqueous phase diagrams of temperature (T) vs protein volume fraction (ϕ) or concentration (C) for the four γ-Crystallins.[17] The region above the coexistence curve represents a single-phase region, and that below the coexistence curve represents a two-phase region. The critical temperature T_c provides a key parameter because it represents the maximum phase-separation temperature. Addition of a pharmacological agent that can lower T_c below the body temperature can reduce protein aggregation in the eye.

In the critical region (within 10 °C of T_c), the coexistence curves can be fitted by the scaling relation

$$\left|\frac{C_c - C}{C_c}\right| = J\left|\frac{T_c - T}{T_c}\right|^{\beta} \tag{4-2}$$

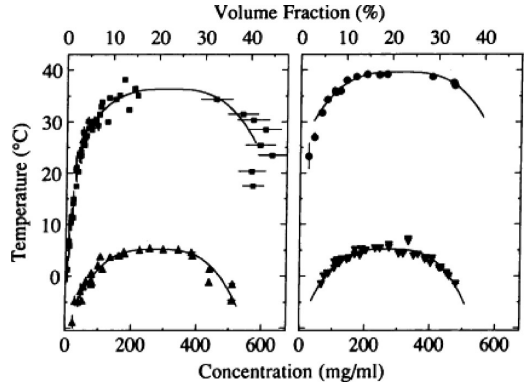

Figure 4-2. Coexistence curves for aqueous solutions of γ_{IIIa} (γ_C) (upper left, ■), γ_{IIIB} (γ_D) (lower left, ▲), γ_{IVa}(γ_E) (upper right, ●), and γ_{II} (γ_B) (lower right,▼) Crystallins. The solid lines represent fits to eq 4-2. Adapted from ref 17.

where C_c is the critical protein concentration; T_c is the absolute critical temperature; exponent $\beta = 0.325$ follows from the three-dimensional Ising model; and J is a parameter that characterizes the width of the coexistence curve. C_c and J are nearly identical for all four binary aqueous γ-Crystallin solutions with a $C_c = 289 \pm 20$ mg/mL and $J = 2.6 \pm 0.1$. The Ising exponent β gives a much better fit than that obtained by using the mean field (classical) exponent $\beta = 0.5$.[17]

To understand interactions in a binary protein−water mixture, Taratuta et al.[18] presented a molecular thermodynamic perturbation model where the reference system is an assembly of hard spheres dispersed in the continuous aqueous phase. The Gibbs free energy G for this system is given by

$$\frac{G}{V} = \frac{G_o}{V} + \frac{k_B T}{\Omega_P}\left[\varphi \ln \varphi - \frac{\varphi - 6\varphi^2 + 4\varphi^3}{(1-\varphi)^2}\right] - \frac{k_B T}{\Omega_P} U\varphi^2 \quad (4\text{-}3)$$

where V is the volume of the solution; G_o is the standard Gibbs free energy; Ω_P is the volume of a protein molecule; k_B is Boltzmann's constant; T is absolute temperature; φ is the volume fraction of protein; and U is a dimensionless parameter that quantifies aqueous protein−protein, protein−water, and water−water interactions. G_o is linear in φ, and it is a measure of the Gibbs energy change of the solution when a single protein molecule is added to a pure solvent. The second term follows from the well-known Carnahan−Starling equation; it represents the entropy of mixing for hard spheres. The last term gives the mean-field approximation of the dissolved protein particles. The model shown in eq 4-3 for binary solutions predicts the critical volume fraction as 13%, while the mean experimental volume fraction for the four binary mixtures was 20.5%.

Because cataract formation in the eye is due to the interaction of several different lens proteins, a study of multicomponent aqueous−protein solutions is useful for understanding the parameters that influence phase separation. Liu et al.[19] have extensively studied aqueous two-protein solutions to obtain the phase separation temperatures as a function of overall protein volume fraction and protein composition. Figure 4-3 shows the phase separation temperature as a function of the total protein volume fraction at different fixed compositions for the aqueous two-protein solution containing γ_{IIIa} and γ_{IIIB} Crystallins. Liu et al.[19] present a molecular-thermodynamic model for an aqueous mixture containing more than one protein. Liu's study of such ternary systems has shown that a native γ_s Crystallin may play a significant role in maintaining transparency of the eye lens.[20] Figure 4-4 shows that the critical phase-separation

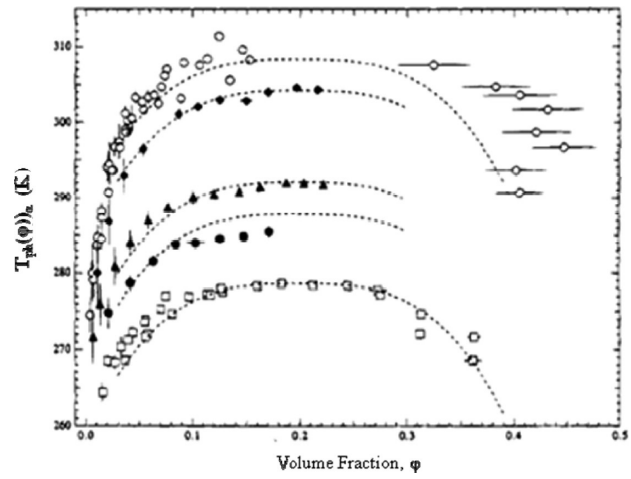

Figure 4-3. Sections of the coexistence surface for aqueous two-protein solutions of γ_{IIIa} and γ_{IIIb} Crystallin at different fixed compositions, α, defined as the ratio of the number of γ_{IIIa} Crystallin molecules to the total number of protein molecules. Experimentally determined points correspond to $\alpha = 0.0$ (□), $\alpha = 0.18$ (●), $\alpha = 0.28$ (▲), $\alpha = 0.64$ (♦), and $\alpha = 1.0$ (○). The dotted curves represent theoretical predictions. Adapted from ref 19.

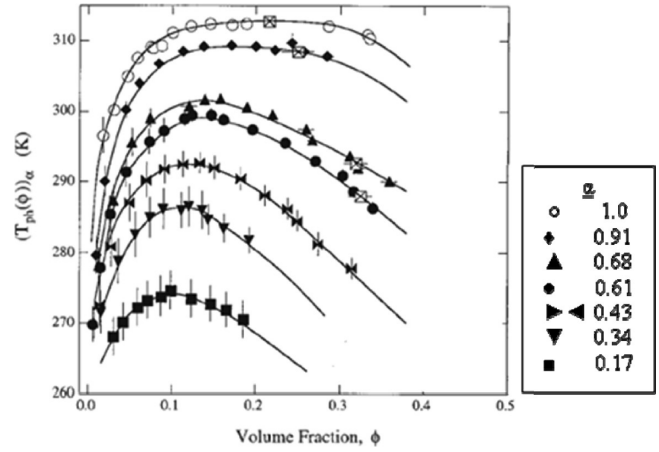

Figure 4-4. Sections of the coexistence surface for aqueous two-protein solutions of γ_{IVa} and γ_s Crystallin at different fixed compositions, α, defined as the ratio of the number of γ_{IVa} Crystallin molecules to the total number of protein molecules. The solid curves show trends in the experimental data. The critical temperature decreases as the fraction of γ_s Crystallin in the aqueous two-protein solution increases. Adapted from ref 20.

temperature of aqueous γ_{IVa} Crystallin in the presence of γ_s Crystallin is substantially reduced at high total volume fractions.

The purpose of a small-molecule cataract inhibitor is to reduce the energy of attraction between the eye-lens proteins. Several small-molecule inhibitors have been proposed in the literature that reduce condensation of the lens proteins. One such chemical inhibitor is oxidized glutathione (SSG) that forms a disulfide complex with γ_{IVa} Crystallin. Figure 4-5 shows that upon addition of SSG the phase-separation temperature of the γ_{IVa} Crystallin−SSG complex is significantly lower than that of γ_{IVa} Crystallin without SSG.[15] Because SSG reduces attraction between Crystallin molecules, it decreases their tendency to aggregate.

This example illustrates how liquid-liquid phase-equilibrium thermodynamics can contribute to a possible therapy for preventing cataracts.

Example 5. Calculation of Biomass Yield from Gibbs Energy Dissipation

In a typical biochemical process, microbes are used to produce a desired product. Thermodynamics can sometimes help to

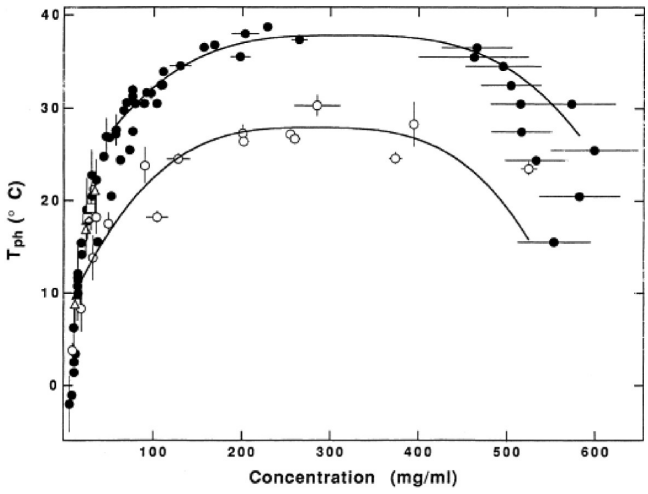

Figure 4-5. Upper curve: the coexistence curve for γ_{IVa} Crystallin. Lower curve: the coexistence curve for γ_{IVa} Crystallin when SSG is added to the solution. Unlike the upper curve, the lower curve has a maximum below body temperature. Therefore, addition of SSG to the eye can prevent cataract formation. Adapted from ref 15.

predict the yield of that product. In a typical application, we want to make biomass that may be produced by cells, or it may be the cells themselves, depending on whether the product is expelled or retained within the cell. As in any chemical reaction, the product yield is related to the Gibbs energy dissipation. Following the discussion by von Stockar et al.,[21] this relationship is best shown by an example.

Methanobacterium thermoautotrophicum is an anaerobic bacterium that generates the energy required for biomass synthesis by methanogenesis, a process that converts H_2 and CO_2 to CH_4, H_2O, and biomass. In an aqueous broth, the growth of biomass is described by

$$H_2 + Y_{C/D}CO_2 + Y_{C/D}NH_3 \rightarrow Y_{X/D}CH_{1.68}O_{0.39}N_{0.24} + Y_{P/D}CH_4 + Y_{W/D}H_2O \quad (5\text{-}1)$$

where D, C, N, X, P, and W stand for H_2, CO_2, NH_3, biomass, CH_4, and H_2O, respectively. NH_3 provides the microbes' need for nitrogen. $Y_{i/D}$ is called the yield coefficient for reactant or product i, defined as the ratio of the moles of component i to the moles of component D. In eq 5-1, yield coefficients are identical to stoichiometric coefficients. The elemental composition of the biomass is obtained experimentally.

The biomass yield, $Y_{X/D}$, is related to the Gibbs energy of dissipation per C-mol biomass produced, equivalent to $\Delta_r G_X$, the Gibbs energy of reaction per C-mol biomass produced

$$\Delta_r G_X = \frac{\Delta_r G_D}{Y_{X/D}} = \frac{1}{Y_{X/D}}\left[\Delta_C G^*_{D,aq} + \frac{y_D}{y_P}(\Delta_c G^*_{c,aq} - \Delta_c G^*_{P,aq})\right] - \left[(\Delta_c G^*_{X,aq} - \Delta_c G^*_{c,aq}) + \frac{y_X}{y_P}(\Delta_c G^*_{c,aq} - \Delta_c G^*_{P,aq})\right] \quad (5\text{-}2)$$

A C-mol refers to the number of moles of carbon. Thus, there are six C-moles in one mole of benzene. From eq 5-2, $Y_{X/D}$ can be calculated for a given $\Delta_r G_X$. In general, to estimate the biomass yield coefficient from eq 5-2, $\Delta_r G^o_X$ is obtained from correlations. Heijnen and van Dijken[22] established a correlation for chemotrophs, that is, for microbes that obtain energy from a chemical source

$$-\Delta_r G^o_X = 200 + 18(6 - n_c)^{1.8} + \exp\{[(3.8 - y_C)^2]^{0.16}(3.6 + 0.4n_c)\} \quad (5\text{-}3)$$

For chemotrophs with reverse electron transport, the following correlation was proposed

$$-\Delta_r G^o_X = 3500 \quad (5\text{-}4)$$

where $\Delta_r G^o_X$ is in kJ/C-mol. γ_C and n_c are the degree of reduction and the number of carbon atoms of the carbon source, respectively.

Liu et al.[23] proposed a simple correlation for $\Delta_r G^o_X$

$$\Delta_r G^o_X = \frac{-666.2}{y_D - 243.1} \quad (y_D \le 4.67) \quad (5\text{-}5a)$$

$$\Delta_r G^o_X = -157y_D + 339 \quad (y_D > 4.67) \quad (5\text{-}5b)$$

$$-\Delta_r G^o_X = -3500 \text{ (for chemotrophs with reverse electron transport)} \quad (5\text{-}5c)$$

where $\Delta_r G^o_X$ is in kJ/C-mol and γ_D is the degree of reduction of the electron donor.

The other terms in eq 5-2, defined below, can be calculated if the following data are obtained experimentally or from the literature:

1. Concentrations of H_2, CO_2, and CH_4 in the off-gas are obtained experimentally using gas chromatography.
2. Henry's constants (H) for H_2,CH_4, and CO_2 in water.
3. Standard Gibbs energies of combustion in the gaseous phase for all components. [The Gibbs energy of combustion for biomass is obtained based on a correlation presented by Sandler et al.[24]]

Knowing the gas phase partial pressures p_i and Henry's constants H_i, the aqueous phase concentrations are obtained from

$$c_i = \frac{p_i}{H_i} \quad (i = CH_4, H_2, CO_2) \quad (5\text{-}6)$$

The cell wall of the bacterium is taken as the boundary for the system wherein H_2 and CH_4 are in a dilute aqueous solution. The Gibbs energies of combustion for H_2 and CH_4 in the aqueous state are given by

$$\Delta_c G_{i,aq} = \Delta_c G^o_{i,aq} + RT \ln c_i \quad (i = CH_4, H_2, CO_2) \quad (5\text{-}7)$$

where $\Delta_c G^o_{i,aq}$ is the standard aqueous phase Gibbs energy of combustion and c_i is the concentration of component i in the dilute aqueous solution. Equation 5-7 does not require an activity coefficient because at normal pressures the solubilities of H_2, CH_4, and CO_2 in the aqueous solution are very small.

Using standard thermodynamics, we obtain

$$\Delta_c G^o_{i,aq} = \Delta_c G^o_{i,g} + RT \ln H_i \quad (5\text{-}8)$$

Knowing the concentrations of H_2, CH_4, and CO_2 in the aqueous phase (c_i) and calculating the standard Gibbs energy of combustion in the aqueous phase ($\Delta_c G^o_{i,aq}$) from eq 5-8, the Gibbs energy of combustion in the aqueous phase ($\Delta_c G_{i,aq}$) can be calculated from eq 5-7. Because the standard Gibbs energies are generally much larger than the concentration-dependent term, this concentration-dependent term can often be neglected without significant loss of accuracy. Thus, the Gibbs energy of reaction (also called Gibbs energy of dissipation) for the reaction in eq 5-1, denoted by $\Delta_r G_D$, is

$$\Delta_c G_D = \Delta_c G^*_{D,aq} + Y_{C/D}\Delta_c G^*_{C,aq} - (Y_{X/D}\Delta_c G^*_X + Y_{P/D}\Delta_c G^*_{P,aq}) \quad (5\text{-}9)$$

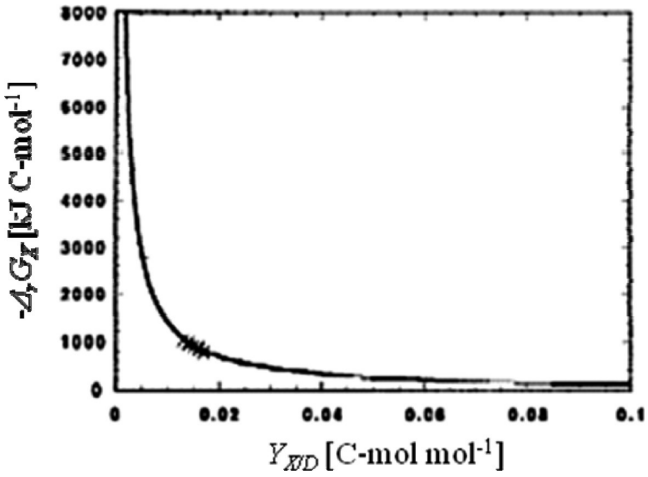

Figure 5-1. Gibbs energy dissipation (kJ per C-mol biomass formed) as a function of $Y_{X/D}$ (C-mol of biomass formed per mole of H_2) for the reaction shown in eq 5-1 at 333 K. (×) denotes experimentally determined biomass yields. Adapted from ref 21.

where superscript * indicates that instead of N_2, NH_3 is chosen as the reference state for the Gibbs energies of combustion. To relate the yield coefficients in eq 5-9 to each other, we use an elemental mass balance and a degree of reductance balance. The degree of reductance (γ) for a compound is defined as the moles of electrons available (per gram of atom carbon) for transfer to oxygen for combustion to CO_2, H_2O, and N_2. For any combustible substance, the degree of reductance is the number of equivalents of available electrons per gram of atom of carbon of that substance. The number of equivalents of available electrons is 4 for carbon, 1 for hydrogen, −2 for oxygen, and −3 for nitrogen. On the basis of these definitions, the degrees of reductance for the compounds in this system are

$$y_D = 2(1) = 2 \tag{5-10a}$$

$$y_C = 1(4) + 2(-2) = 0 \tag{5-10b}$$

$$y_N = 1(-3) + 3(1) = 0 \tag{5-10c}$$

$$y_X = 1(4) + 1.68(1) + 0.39(-2) + 0.24(-3) = 4.18 \tag{5-10d}$$

$$y_P = 1(4) + 4(1) = 8 \tag{5-10e}$$

$$y_W = 2(1) + 1(-2) = 0 \tag{5-10f}$$

The degree of reductance balance is obtained from conservation of available electrons

$$y_D + Y_{C/D}y_C + Y_{N/D}y_N = Y_{X/D}y_X + Y_{P/D}y_P + Y_{W/D}y_W$$

$$y_D = Y_{X/D}y_X + Y_{P/D}y_P$$

$$Y_{P/D} = \frac{y_D}{y_P} - \frac{y_X}{y_P}Y_{X/D} \tag{5-11}$$

An elemental-carbon balance for the system gives

$$Y_{C/D} = Y_{X/D} + Y_{P/D} \tag{5-12}$$

Combining eqs 5-9, 5-11, and 5-12 gives the required relation between the biomass yield and the Gibbs energy of dissipation per C-mol biomass produced, as shown in eq 5-2.

Figure 5-1 shows the calculated relation between the Gibbs energy of dissipation and the desired yield coefficient $Y_{X/D}$. For a biomass yield, $Y_{X/D} \sim 0.015$ mol/mol of H_2, and a mass balance gives the other yields in units of mol/mol H_2

$$Y_{N/D} = 3.6 \times 10^{-3}$$
$$Y_{C/D} = 0.2572$$
$$Y_{P/D} = 0.2422$$
$$Y_{W/D} = 0.5085$$

Thus, for every mole of H_2 consumed, the microbe produces 0.2422 mol of CH_4. Figure 5-1 shows a frequently observed result that the experimental biomass yields are closely clustered together in the middle, rather than at the extremes. A qualitative explanation for this result is provided by splitting eq 5-1 into two reactions—catabolism and anabolism.[25]

Catabolism

$$H_2 + aCO_2 \rightarrow bCH_4 + cH_2O \quad \Delta G_{cat} \tag{5-13a}$$

Anabolism

$$dCH_4 + eH_2O + Y_{N/D}NH_3 \rightarrow Y_{X/D}X + fCO_2 \quad \Delta G = X_{Y/D}\Delta G_{ana} \tag{5-13b}$$

where, for eqs 5-13a and 5-13b, ΔG_{cat} is the Gibbs energy of reaction per C-mol of H_2 for catabolism and ΔG_{ana} is the Gibbs energy of reaction per C-mol biomass produced for anabolism. Here, a through f are stoichiometric coefficients for the catabolism and anabolism reactions; ΔG_{cat} and ΔG_{ana} are related to the overall Gibbs energy of reaction (or Gibbs energy of dissipation) by

$$\Delta_r G_D = \Delta G_{cat} + Y_{X/D}\Delta G_{ana} \tag{5-14}$$

Catabolism is an energy-producing reaction, with a negative ΔG_{cat}, and anabolism is an endothermic reaction with a positive ΔG_{ana}. In an inefficient growth system (where $|\Delta G_{cat}| \gg |\Delta G_{ana}|$), the Gibbs energy of dissipation is also a large negative quantity, and eq 5-14 tells us that the biomass yield is small and not desirable for the microbe. At the other extreme, an efficient growth system (where $|\Delta G_{ana}| \gg |\Delta G_{cat}|$), the biomass yields are optimal; however, the Gibbs energy of dissipation is small and hence the rate of the overall reaction is likely to be slow. A slow reaction rate is undesirable because under these conditions the microbe will be outgrown by competitors. Hence, microbes have possibly evolved to have a $\Delta_r G_X$ and $Y_{X/D}$ somewhere in between the two extremes of inefficient growth (very high $|\Delta_r G_X|$ and very low $Y_{X/D}$) and efficient growth (very low $|\Delta_r G_X|$ and very high $Y_{X/D}$), as indicated in Figure 5-1.

von Stockar et al. and others have presented analyses similar to that above for a variety of relatively simple bioreactions using a large number of aerobic and anaerobic microbes. These analyses indicate that thermodynamics may provide good estimates of the biomass yield for simple microbial systems, but further developments are required to apply these methods to complex mammalian cell cultures.

Example 6: Prevention of Liquid−Liquid Phase Separation in Freeze-Concentrated Formulations for Protein Lyophilization

Freeze-drying (lyophilization) is a process for removing water from a solution in the form of ice; the advantage of this process is that it produces a nearly anhydrous solute. Freeze-drying is a popular method of drying in the pharmaceutical industry because it increases the shelf life of a drug. Freeze-drying

enhances the chemical stability of biomolecules. Aqueous biomolecules are susceptible to numerous unwanted reactions like hydrolysis, cross-linking, oxidation, aggregation, and disulfide rearrangements.[26] In any drying process, it is necessary to prevent protein denaturing. To increase the stability of a protein in solution, it is common practice to add excipients to the solution. Excipients are also used to promote stabilization of freeze-dried proteins. However, the formation of ice during freeze-drying increases the concentration of excipients in the liquid. Unlike dilute solutions, the high concentration of excipients during freeze-drying increases the tendency for undesired liquid−liquid phase separation. Phase separation of these excipients into two phases can denature the protein. Because phase separation must be avoided, it is useful to determine the conditions when such separation is likely. As shown by Randolph and co-workers, thermodynamics provides guidance toward determining those conditions.[27]

For a dilute or semidilute aqueous system with two polymeric excipients, denoted by subscripts 2 and 3, and water denoted by subscript 1, the chemical potentials (μ) for the excipients are given by

$$\mu_2 - \mu_2^0 = RT(\ln m_2 + a_{22}m_2 + a_{23}m_3) \qquad (6\text{-}1)$$

$$\mu_3 - \mu_3^0 = RT(\ln m_3 + a_{33}m_3 + a_{23}m_2) \qquad (6\text{-}2)$$

where m_i is the molal concentration of polymer i and superscript 0 indicates the (infinite-dilution) standard state chemical potential; a_{22}, a_{33}, and a_{23} are coefficients that characterize 2−2, 3−3, and 2−3 interactions. The chemical potential of water is calculated by combining eqs 6-1 and 6-2 with the Gibbs−Duhem equation

$$\mu_1 - \mu_1^0 = -RTV_1\rho_1\left(m_2 + m_3 + \frac{a_{22}}{2}(m_2)^2 + \frac{a_{33}}{2}(m_3)^2 + a_{23}m_2m_3\right) \qquad (6\text{-}3)$$

where V_1 and ρ_1 are the molar volume and mass density of pure water, respectively, and μ_1^0 is the standard-state chemical potential of pure water at temperature T. The interaction parameters are obtained from second virial coefficients B that can be obtained from osmotic-pressure or laser-light scattering data

$$2B_{22} = 1000\frac{a_{22}}{(M_2)^2} \qquad (6\text{-}4a)$$

$$2B_{33} = 1000\frac{a_{33}}{(M_3)^2} \qquad (6\text{-}4b)$$

$$2B_{23} = 1000\frac{a_{23}}{M_2M_3} \qquad (6\text{-}4c)$$

where M_i is the molecular weight of polymer i.

In a two-phase system at equilibrium, the chemical potential of each component in phase ′ is equal to that in phase ″

$$\mu_1' = \mu_1''; \mu_2' = \mu_2''; \mu_3' = \mu_3'' \qquad (6\text{-}5)$$

Coupled with mass balances, eqs 6-1, 6-2, 6-3, and 6-5 give the binodal curve. For practical calculations, it is more convenient to obtain the spinodal curve given by Gibbs' stability criterion

$$\left(\frac{\partial\mu_2}{\partial n_2}\right)_{T,p,n_1,n_2}\left(\frac{\partial\mu_3}{\partial n_3}\right)_{T,p,n_1,n_2} - \left(\frac{\partial\mu_2}{\partial n_3}\right)^2_{T,p,n_1,n_2} = 0 \qquad (6\text{-}6)$$

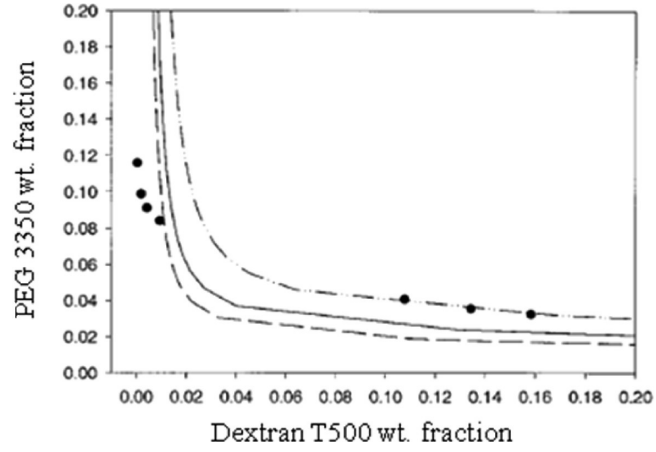

Figure 6-1. Calculated spinodal curve for PEG3350 and dextran T500. Points are experimental data. Adapted from ref 27.

where n_i is the number of moles of component i.

In freeze-drying, when the solution is cooled, ice is formed, and the aqueous-phase concentration of the excipients increases. At temperature T, when equilibrium is attained, the chemical potential of ice is equal to that of liquid water

$$\mu_{ice}(T) = \mu_1(T, m_2, m_3) \qquad (6\text{-}7)$$

Equation 6-7, along with those given above, can be used to calculate the concentration of the excipients when phase separation occurs at temperature T. At this temperature, the change in chemical potential in going from pure liquid water to ice is given by

$$\mu_{ice}(T) - \mu_1^0(T) = \frac{-\Delta H}{T_f}(T - T_f) - (C_{p_{ice}} - C_{p_{water}}) \cdot \left[T\ln\left(\frac{T}{T_f}\right) - (T - T_f)\right] \qquad (6\text{-}8)$$

where T_f is the freezing temperature of pure water (273 K) and C_p^{ice} and C_p^{liq} are the heat capacities of ice and pure supercooled liquid water, respectively; μ_1^0 is the standard state chemical potential of pure water at T; and ΔH is the enthalpy of fusion.

The equations above represent the thermodynamic limit. However, in practice, because the supercooled phase is very viscous, components cannot move easily from one phase to another. Phase separation is restrained by the slow rate of diffusion of water molecules from one phase to another, as shown by a curve of transition temperature as a function of temperature on the phase diagram.

Figure 6-1 shows the spinodal curve as a function of weight fraction of commonly used excipients, PEG3350 and dextranT500. Upon freeze-drying, Randolph et al.[27] show that the concentrations of the excipients rise, but the weight ratio of the two excipients remains the same. Figure 6-2 shows a plot of temperature vs the weight ratios of PEG/dextran. The transition temperature at any weight ratio of PEG and dextran determines the minimum temperature for phase separation, although thermodynamics favors phase splitting at lower termperatures. Thus, the shaded region in Figure 6-2 represents the region where undesired phase separation is likely to occur. Figure 6-3 shows a phase diagram for a similar system containing the excipients PEG and albumin. Because the transition curve is above the spinodal curve for all considered weight ratios, Figure 6-3 implies that phase separation does not occur for this system.

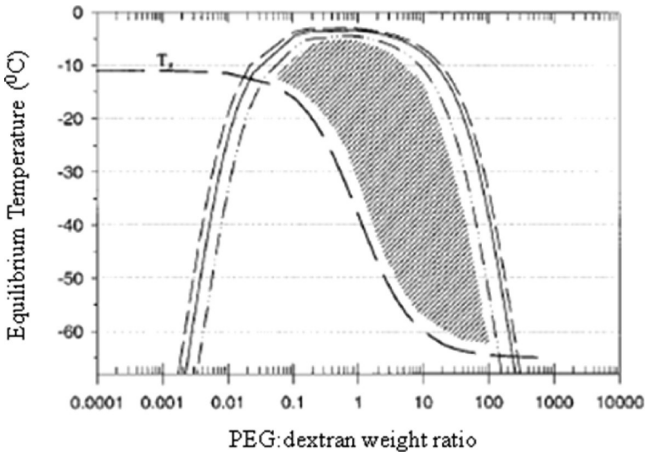

Figure 6-2. Subzero temperature (°C) is necessary to achieve phase-separating concentrations in a thermodynamically equilibrated frozen solution of PEG 3350 and dextran T500. Curves correspond to spinodals in Figure 6-1. The dashed T_g line represents an approximate transition temperature. The shaded envelope region represents phase separation. Adapted from ref 27.

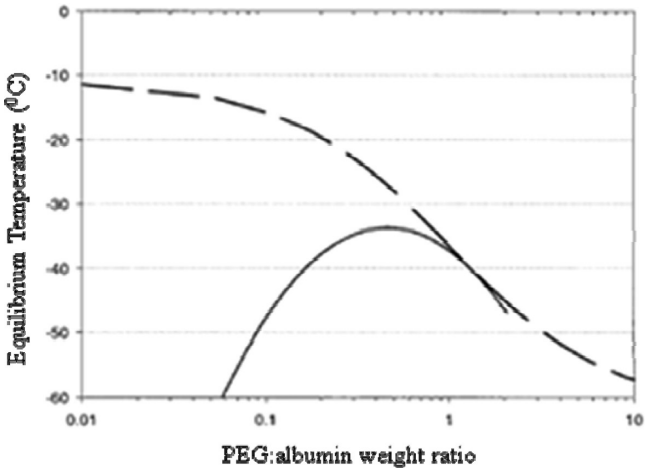

Figure 6-3. Equilibrium temperatures necessary to achieve phase-separating concentrations in a frozen solution of PEG and albumin. The glass transition is represented by a dashed line. Because the glass transition is reached before attaining concentrations sufficient to induce phase-separation, a phase-separation envelope does not exist for PEG/albumin in contrast to the PEG/dextran mixture. Adapted from ref 27.

Because we want to avoid phase separation, Figure 6-3 suggests that excipients PEG and albumin are preferable to PEG and dextran.

Randolph et al.[27] obtained Scanning Electron Microscopy (SEM) images for the PEG/dextran system for different weight ratios. SEM images showed that for a weight ratio of 1 two condensed phases are present, suggesting that phase separation has occurred. However, at lower or higher weight ratios, only one phase is observed.

To determine the effect of phase separation on the stability of protein structure, Randolph et al.[27] used infrared spectroscopy to obtain the loss of native structure of hemoglobin. Figure 6-4 shows how the width of a characteristic peak of hemoglobin at 1655 cm^{-1} changes with loss of structure. In this case, freeze-drying of hemoglobin was studied for different weight ratios of PEG and dextran as excipients. Prior to drying, the system was annealed at −7 °C for 1 h in one case and 12 h in the other. The loss of native structure of the protein is shown in Figure 6-5 for different weight ratios. For those weight ratios where phase separation occurs, we expect a change in the

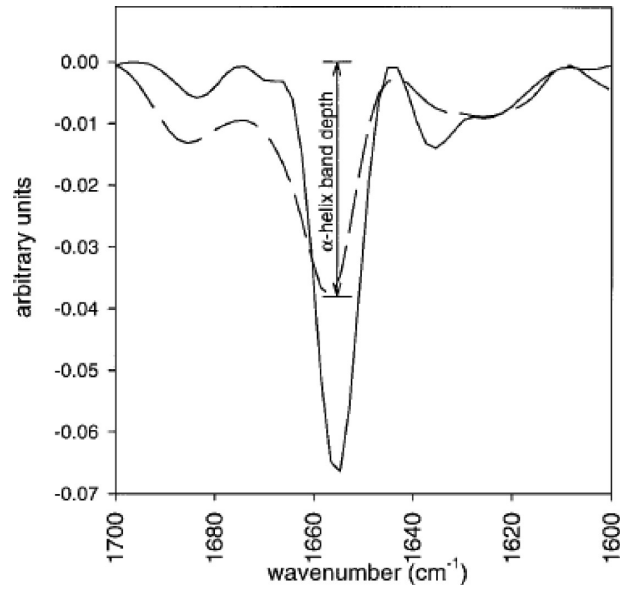

Figure 6-4. Infrared spectrum of hemoglobin in aqueous solution shown by a solid line. A dashed line shows the infrared spectrum in the dried state, freeze-dried in 4% PEG 3350 and 4% dextran T500. The reduced α-helix band depth shows the loss of native structure due to freeze-drying. Adapted from ref 27.

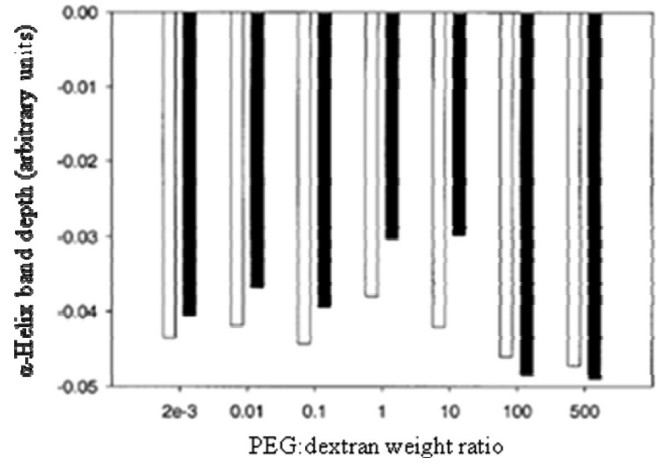

Figure 6-5. Depth of α-helix band from infrared spectra of dried hemoglobin with different PEG:dextran weight ratios. Samples that were annealed for 1 h at −7 °C prior to drying are shown by white bars, and samples that were annealed for 12 h are shown in black. Adapted from ref 27.

structure of the protein; therefore, we anticipate significant differences in the width of the band obtained for 1 h compared to 12 h annealing. This difference is verified by results shown in Figure 6-5 that show, for weight ratios close to 1, there are significant differences in the width of the band. Also, SEM images show that this is the weight ratio where phase separation occurs. The experimental results indicate that phase separation is correlated with protein denaturation as predicted in Figure 6-2. This figure shows that at −7 °C weight ratios close to 1 fall within the phase separation envelope that is detrimental to protein structure.

This example shows that thermodynamic analysis can provide a useful tool for predicting the region where undesired phase separation may occur during freeze-drying. Thermodynamic analysis can help find the optimal conditions where phase separation can be avoided. Thermodynamic analysis can reduce

the amount of experimental work that would be required in the absence of thermodynamic calculations.

Conclusion

The examples shown here illustrate how chemical thermodynamics provides a useful tool for biotechnology. In each example, thermodynamics provides a theoretical framework for contributing toward an answer to a biotechnical problem. Coupled with insights from molecular physics and with limited suitable experimental data, the framework can lead to useful results.

The generality and versatility of thermodynamics allow application to all materials, no matter how complex. Those who seek new applications of thermodynamics need not exclude biomacromolecules; they too are subject to the laws of thermodynamics.

Nearly 90 years ago, Gilbert Lewis and Merle Randall published a pioneering book (*Thermodynamics and the Free Energy of Substances*) that showed how the abstract chemical thermodynamics of Gibbs can be applied to real solids and fluids. Once again, we can be inspired by the famous introduction:

> *Let this book be dedicated to the chemists of the newer generation, who will not wish to reject all inferences from conjecture or surmise, but who will not care to speculate concerning that which may be surely known. The fascination of a growing science lies in the work of the pioneers at the very borderland of the unknown, but to reach this frontier one must pass over well-traveled roads; of these one of the safest and surest is the broad highway of thermodynamics.*

Literature Cited

(1) Liu, C.; Kamai, D. T.; King, J. A.; Wang, D. I. C.; Blankschtein, D. Separation of Proteins and Viruses Using Two-phase Aqueous Micellar Systems. *J. Chromatogr., B: Biomed.* **1998**, *711*, 127.

(2) Nikas, Y. J.; Liu, C.; Srivastava, T.; Abbott, N. L.; Blankschtein, D. Protein Partitioning in Two-phase Aqueous Nonionic Micellar Solutions. *Macromolecules* **1992**, *25*, 4797.

(3) Kamai, D. T.; Liu, C.; Haase-Pettingell, C.; King, J. A.; Wang, D. I. C.; Blankschtein, D. Understanding Viral Partitioning in Two-phase Aqueous Nonionic Micellar Systems: 1. Role of Attractive Interactions Between Viruses and Micelles. *Biotechnol. Bioeng.* **2002**, *2*, 190.

(4) Kamai, D. T.; King, J. A.; Wang, D. I. C.; Blankschtein, D. Understanding Viral Partitioning in Two-phase Aqueous Nonionic Micellar Systems: 2. Effect of Entrained Micelle-Poor Domains. *Biotechnol. Bioeng.* **2002**, *2*, 203.

(5) Ohtaka, H.; Freire, E. Adaptive Inhibitors of the HIV-1 Protease. *Prog. Biophys. Mol. Biol.* **2005**, *88*, 193.

(6) Tavares, F. W.; Bratko, D.; Striolo, A.; Blanch, H. W.; Prausnitz, J. M. Phase Behavior of Aqueous Solutions Containing Dipolar Proteins from Second-Order Perturbation Theory. *J. Chem. Phys.* **2004**, *120*, 9859.

(7) Tavares, F. W.; Prausnitz, J. M. Analytic Calculation of Phase Diagrams for Solutions Containing Colloids or Globular Proteins. *Colloid Polym. Sci.* **2004**, *282*, 620.

(8) Velasco, E.; Mederos, L. Equation of State of the Hard-Disc Solid. *Phys. Rev. B* **1997**, *56*, 2432.

(9) Boström, M.; Craig, V. S. J.; Albion, R.; Williams, D. R. M.; Ninham, B. W. Hofmeister Effects in pH Measurements: Role of Added Salt and Co-Ions. *J. Phys. Chem. B* **2003**, *107*, 2875.

(10) Tavares, F. W.; Bratko, D.; Blanch, H. W.; Prausnitz, J. M. Ion-Specific Effects in the Colloid-Colloid or Protein-Protein Potential of Mean Force: Role of Salt-Macroion van der Waals Interactions. *J. Phys. Chem. B* **2004**, *108*, 9228.

(11) Collins, K. D.; Neilson, G. W.; Enderby, J. E. Ions in water: characterizing the forces that control chemical processes and biological structure. *Biophys. Chem.* **2007**, *128*, 95.

(12) Athawale, M. V.; Jamadagni, S. N.; Garde, S. How hydrophobic hydration responds to solute size and attractions: Theory and simulations. *J. Chem. Phys.* **2009**, *131*, 115102.

(13) Hummer, G.; Garde, S.; García, A. E.; Pratt, L. R. New perspectives on hydrophobic effects. *Chem. Phys.* **2000**, *258*, 349.

(14) Rasaiah, J. C.; Garde, S.; Hummer, G. Water in nonpolar confinement: From nanotubes to proteins and beyond. *Annu. Rev. Phys. Chem.* **2008**, *59*, 713.

(15) Benedek, G. B.; Pande, J.; Thurston, G. M.; Clark, J. I. Theoretical and Experimental Basis for the Inhibition of Cataracts. *Prog. Retinal Eye Res.* **1999**, *18*, 391.

(16) Thurston, G. M.; Hayden, D. L.; Burrows, P.; Clark, J. I.; Taret, V. G.; Kandel, J.; Courogen, M.; Peetermans, J. A.; Bowen, M. S.; Miller, D.; Sullivan, K. M.; Storb, R.; Stern, H.; Benedek, G. B. Quasielastic Light Scattering Study of the Living Human Lens as a Function of Age. *Curr. Eye Res.* **1997**, *16*, 197.

(17) Broide, M. L.; Berland, C. R.; Pande, J.; Ogun, O. O.; Benedek, G. B. Binary-liquid Phase Separation of Lens Protein Solutions. *Proc. Natl. Acad. Sci. U.S.A.* **1991**, *88*, 5660.

(18) Taratuta, V. G.; Holschbach, A.; Thurston, G. M.; Blankschtein, D.; Benedek, G. B. Liquid-liquid Phase Separation of Aqueous Lysozyme Solutions: Effects of pH and Salt Identity. *J. Phys. Chem.* **1990**, *94*, 2140.

(19) Liu, C.; Lomakin, A.; Thurston, G. M.; Hayden, D.; Pande, A.; Pande, J.; Ogun, O.; Asherie, N.; Benedek, G. B. Phase Separation in Multicomponent Aqueous-protein Solutions. *J. Phys. Chem.* **1995**, *99*, 454.

(20) Liu, C.; Asherie, N.; Lomakin, A.; Pande, J.; Ogun, O.; Benedek, G. B. Phase Separation in Aqueous Solutions of Lens γ- crystallins: Special Role of γ_s. *Proc. Natl. Acad. Sci. U.S.A.* **1996**, *93*, 377.

(21) Schill, N. A.; Liu, J.-S.; von Stockar, U. Thermodynamic Analysis of Growth of *Methanobacterium thermoautotrophicum*. *Biotechnol. Bioeng.* **1999**, *64*, 74.

(22) Heijnen, J. J.; van Dijken, J. P. In Search of a Thermodynamic Description of Biomass Yields for the Chemotrophic Growth of Microorganisms. *Biotechnol. Bioeng.* **1992**, *39*, 833.

(23) Liu, J.-S.; Vojinović, V.; Patiño, R.; Maskow, T.; von Stockar, Y. A Comparison of Various Gibbs Energy Dissipation Correlations for Predicting Microbial Growth Yields. *Thermochim. Acta* **2007**, *458*, 38.

(24) Sandler, S. I.; Orbey, H. On the Thermodynamics of Microbial Growth Processes. *Biotechnol. Bioeng.* **1991**, *38*, 697.

(25) von Stockar, U.; Maskow, T.; Liu, J.; Marison, I. W.; Patino, R. Thermodynamics of Microbial Growth and Metabolism: An Analysis of the Current Situation. *J. Biotechnol.* **2006**, *121*, 517.

(26) Franks, F. Freeze-drying of Bioproducts: Putting Principles into Practice. *Eur. J. Pharm. Biopharm.* **1998**, *45*, 221.

(27) Heller, M. C.; Carpenter, J. F.; Randolph, T. W. Application of a Thermodynamic Model to the Prediction of Phase Separations in Freeze-concentrated Formulations for Protein Lyophilization. *Arch. Biochem. Biophys.* **1999**, *363*, 191.

Received for review March 4, 2010
Revised manuscript received May 28, 2010
Accepted June 2, 2010

IE1004916